Received: 31 December 2017 | Revised: 12 March 2019 | Accepted: 24 March 2019

DOI: 10.1002/asjc.2146

SPECIAL ISSUE

WILEY

Control-oriented modeling and robust nonlinear triple-step controller design for an air-feed system for polymer electrolyte membrane fuel cells

Yunfeng Hu[1,2] | Huan Chen[2] | Xun Gong[1,2,3] | Shuyou Yu[1,2] | Jinwu Gao[1,2] | Hong Chen[1,2]

[1]State Key Laboratory of Automotive Simulation and Control, Jilin University, Changchun, Jilin, China

[2]Department of Control Science and Engineering, Jilin University, Changchun, Jilin, China

[3]School of Artificial Intelligence, Jilin University, Changchun

Correspondence
Xun Gong, State Key Laboratory of Automotive Simulation and Control, Jilin University, Changchun, Jilin 130012, China.
Email: gongxun10@hotmail.com

Funding information
National Natural Science Foundation of China, Grant/Award Number: 61703177 and 11601040; Jilin Provincial Science Foundation of China, Grant/Award Number: 20190302119GX and 20180101037JC; Jilin Provincial Development and Reform Commission Foundation of China, Grant/Award Number: 2019C036-4; Funds for Joint Project of Jilin Province and Jilin University, Grant/Award Number: SXGJSF2017-2-1-1

Abstract

The efficient operation of polymer electrolyte membrane fuel cells (PEMFCs) significantly relies on the reliable control of air-feed system. The core control objective in air-feed system is to track a pre-defined reference of the oxygen excess ratio to avoid oxygen starvation and stack damage. In this paper, we focus on the modeling of the air-feed system in a PEMFC and the robust nonlinear controller design for the oxygen excess ratio tracking control. To facilitate the subsequent nonlinear controller design, a specific affine-like, second-order, control-oriented model of oxygen excess ratio dynamic behavior is developed, and the modeling uncertainty is estimated and compensated by using an extended state observer (ESO). The control-oriented model is verified via a high-fidelity plant model. A nonlinear controller for oxygen excess ratio tracking control is proposed based on the triple-step technique which is robust against the system disturbances. The tuning rule of the controller parameters is discussed in the scheme of the linear system. Finally, simulations are conducted to demonstrate the effectiveness and advantages of the proposed controller under variant operating conditions compared with baseline controllers.

KEYWORDS

air-feed system, control-oriented modeling, nonlinear control, PEMFCs, stability analysis

1 | INTRODUCTION

Concerns of environmental impact and tightened fuel economy regulations have motivated numerous technical innovations for vehicles efficiency improvement, along with the increasing penetration of fuel cell vehicles (FCVs). Polymer electrolyte membrane fuel cells (PEMFCs) technology, directly converting the chemical energy into electrical energy with water byproduct only, is promising for vehicles because of high power density, zero emission and reproducibility [1–3].

The reliable operation of PEMFC is enabled by several auxiliary systems, including an air-feed system, a hydrogen supply system, a water and thermal management system

and a power management system [4]. On one hand, the air-feed system plays an important role on the efficient operation of the PEMFC as it consumes nearly 20% of the total energy in the system [5,6]. On the other hand, the precise quantity of the air supply should be guaranteed because the air starvation caused by insufficient air inflow will reduce the cell life and potentially damage the stack [7,8]. Therefore, it is essential to design a reliable air-feed system control strategy to maintain the desired oxygen excess ratio.

Until now, many control schemes have been applied to air-feed control system. The classical solutions are the proportional-integral-derivative (PID) control [9] and its variants, e.g. neural PID [10] and fuzzy PID [9,11] with improved control performances. For determination of the tracking target, Becherif et al. propose to compute the optimal value for the oxygen stoichiometry reference to maximize the fuel cell output power [12]. In [13], a linear quadratic Gaussian (LQG) regulator is developed for cathode pressure tracking control. In [14], a linear model predictive control (MPC) scheme with multi-objectives is developed to optimize efficiency and avoid oxygen starvation. Due to the complexity of air-feed system, linear models obtained by linearization around a specific operating point are often limited to represent all the nonlinear transients. To deal with the nonlinear characteristics, sliding mode controllers based on a super-twisting algorithm are designed in [15,16]. In [17], a robust control scheme based on adaptive sliding mode feedback control is proposed to control the air stoichiometry, air pressure and relative humidity. In [18], to address the speed fluctuation problem, an heuristic modification of the supertwisting algorithm is proposed and the control performance is validated experimentally. To enforce constraints, a nonlinear MPC scheme is proposed to control the air inflow so as to guarantee the desired oxygen supply in [19]. Although the air-feed system control problem has been extensively studied, several issues still require further consideration and clarification: (i) Due to the high nonlinearity of air-feed system, the nonlinear controller design procedure tends to be so sophisticated that a gap has arisen between the algorithm development in theoretical community and the solutions implementation by engineering practitioners in industry; (ii) Regarding controller tuning, specific parameter tuning rules are required to guide the practical implementation; (iii) A comprehensive closed-loop stability analysis is suggested.

The investigation pursued in this paper is motivated by the need for a robust control solution that addresses issues arising in nonlinear control for the air-feed system with uncertainties and the previous research on the application of triple-step nonlinear control for automotive powertrain control, see [20–22] and references therein. We start by describing the physical structure of a PEMFC and continue by deriving a control-oriented model in an input-output-affine formulation with verified modeling accuracy. We then formulate a nonlinear feedback controller using triple-step method to guarantee the stability and robustness of the closed-loop system. Finally, this paper presents a specific control tuning rule and addresses the potential issues towards implementation. The main contributions of this paper are summarized as follows.

- To facilitate the subsequent nonlinear controller design of oxygen excess ratio tracking control, a second-order, affine-like, control-oriented air-feed system model is derived and the modeling accuracy is validated, where a disturbance observer compensates the modeling discrepancies.
- An implementation-oriented robust nonlinear air-feed system controller is designed followed by an intuitive way by using the triple-step method, where the stability and the robustness are guaranteed by the Lyapunov method.
- A specific controller tuning rule is explicitly determined via linear system theory since the closed-loop system is inherently arranged into a linear system following by the sequential design procedures as suggested by triple-step method.

The organization of this paper is as follows. Section II briefly describes the PEMFCs system and presents a control-oriented model of the air-feed system. Section III presents the proposed robust controller design, the stability analysis and the parameter tuning rules. Section IV reports and analyzes the simulation results. Section VI summaries the key findings.

2 | SYSTEM DESCRIPTION AND CONTROL-ORIENTED MODEL

2.1 | System description and control problem statement

The schematic diagram of a PEMFCs system is presented in Figure 1. The safe and reliable operation of PEMFCs are realized by four auxiliary systems including an air-feed system, a hydrogen supply system, a water and thermal management system and a power management system [23]. A brief functional description of these four systems is introduced as follows.

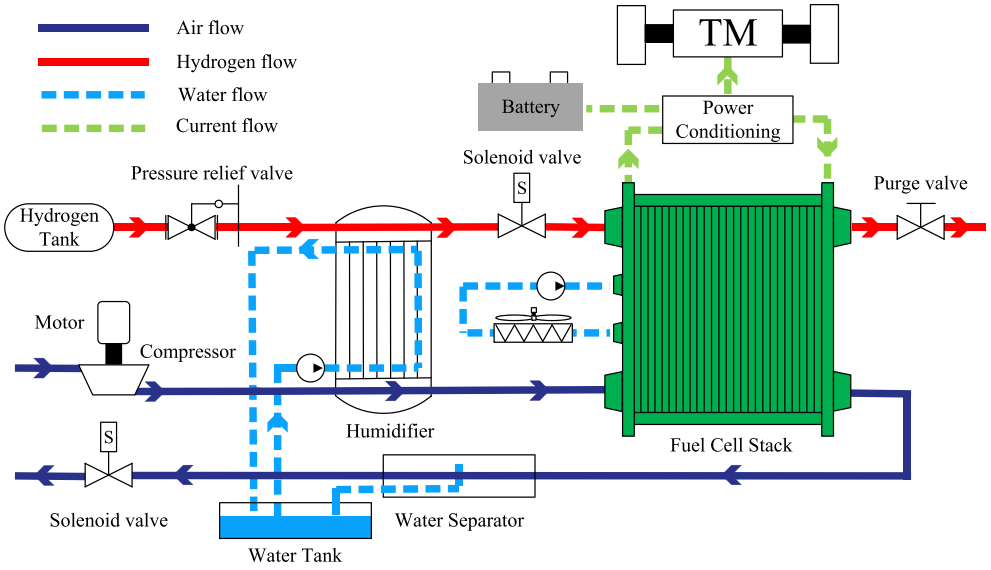

FIGURE 1 Schematic diagram of THE PEMFC system [Color figure can be viewed at wileyonlinelibrary.com]

1. Air-feed system: This system provides the oxygen flow to PEMFCs stack for the electrochemical reactions, where the air flow in the cathode is adjusted by an electric-driven compressor to achieve the desired oxygen excess ratio.
2. Hydrogen supply system: This system provides the hydrogen flow to PEMFCs stack for the electrochemical reactions, where the hydrogen is induced from a high-pressure hydrogen tank by a pressure release valve and then adjusted into anode by a solenoid valve.
3. Water and thermal management system: This system is to manage the membrane hydration, humidity and stack temperature in the PEMFCs stack. Water injected into the air-path regulates the membrane hydration while the humidifier adjusts the humidity of membrane. The stack temperature is regulated within a suitable range by the cooling system, including a cooling fan and a pump, to guarantee operating safety and reacting efficiency.
4. Power management system. This system manages the power drawn from the PEMFCs. Auxiliary electric power devices are used to process and filter the electricity to ensure smooth power delivery and power demand following.

In this paper, we only focus on the air-feed control system design and assume other systems are well designed. The main control objective is to achieve rapid tracking of a oxygen excess ratio reference with small overshoot and without oscillation. Considering the nonlinearity and the uncertainties in the air-feed system, the triple-step nonlinear controller design technique will be applied. A control-oriented model of the air-feed system is derived in the following section which facilitates the subsequent controller design.

2.2 | Control-oriented model

Based on the the first principle [18,24], the nonlinear dynamics of the air-feed system is expressed by

$$\begin{aligned}\dot{w}_{cp} &= -a_1 w_{cp} + a_2 u - \frac{1}{w_{cp}}(a_3 P_{sm}^l - a_4) W_{cp},\\ \dot{P}_{sm} &= -(a_5 + a_6 P_{sm}^l)(P_{sm} - P_{ca} - a_7 W_{cp}),\\ \dot{P}_{ca} &= -a_8 P_{ca} + a_9 P_{sm} + a_{10} - a_{11} I_{st},\end{aligned} \tag{1}$$

where u denotes the voltage applied to the compressor motor which is the control input, w_{cp} is the angular speed of the compressor, P_{sm} is the supply manifold pressure, and P_{ca} is the cathode pressure, I_{st} is the stack current treated as a measurable disturbance (exogenous input), W_{cp} is the air mass flow through the compressor associated with w_{cp} and P_{sm}, $a_1 \sim a_{11}$ are the system parameters, for details please see Appendix and Table A1. The air mass flow W_{cp} is described by a parametric model [5]

$$W_{cp} = \left[1 - e^{\beta\left(\frac{\psi}{\psi_{max}} - 1\right)}\right] \sum_{j=1}^{5} \alpha_j w_{cp}^j, j = 1, 2, \ldots, 5, \tag{2}$$

where α_j, β, ψ and ψ_{max} are fitted variables given in Table A2 in Appendix.

The oxygen excess ratio is defined as

$$\lambda_{O_2} = \frac{W_{O_2,in}}{W_{O_2,react}} = \frac{c_1(P_{sm} - P_{ca})}{c_2 I_{st}}, \tag{3}$$

where $W_{O_2,in}$ and $W_{O_2,react}$ denote the supplied oxygen mass flow and the consumed oxygen mass flow respectively, coefficients c_1 and c_2 can be found in the Appendix.

According to (3), there exits a disturbance input I_{st} in the denominator of λ_{O_2}. To avoid the mathematical complexity introduced by directly differentiating λ_{O_2} in the controller design process, we treat the pressure difference $P_{sm} - P_{ca}$ as the control output instead of λ_{O_2}. Thus, we define the control output as

$$y = P_{sm} - P_{ca} = \frac{c_2 I_{st}}{c_1}\lambda_{O_2}. \tag{4}$$

Then, differentiating y and combining (1) lead to

$$\begin{aligned}\dot{y} =& \dot{P}_{sm} - \dot{P}_{ca}\\ =& -(a_5 + a_8 + a_6 P_{sm}^l)y + (a_5 + a_6 P_{sm}^l)a_7 W_{cp}\\ & -(a_9 - a_8)P_{sm} - a_{10} + a_{11} I_{st}.\end{aligned} \tag{5}$$

Again, differentiating (5) leads to an affine-like formulation of the model as follows,

$$\ddot{y} = f_1(p)\dot{y} + f_2(y,p)y + f_3(p) + g(p)u + d(t), \tag{6}$$

where $p = [P_{sm}, w_{cp}]$ is the vector of the measurable states in air-feed system, detailed expressions of $f_1(p)$, $f_2(y,p)$, $f_3(p)$ and $g(p)$ are given in (7), and $d(t)$ sums up the modeling and external disturbances. Note that this paper focuses on the air-feed system control in normal fuel cell operating conditions where $w_{cp} \neq 0$. A special start-up control process [25] for $w_{cp} = 0$ is essential and should be carefully designed which is out of the scope in this paper.

$$\begin{aligned}f_1(p) &= -a_5 - a_8 - a_6 P_{sm}^l,\\ f_2(p) &= \left[a_6 l P_{sm}^{l-1} y - 2a_6 a_7 l W_{cp} P_{sm}^{l-1} - (a_5 + a_6 P_{sm}^l)a_7 \frac{\partial W_{cp}}{\partial P_{sm}}\right.\\ &\quad \left. + (a_9 - a_8)\right](a_5 + a_6 P_{sm}^l),\\ f_3(p) &= (a_5 + a_6 P_{sm}^l)a_7 \left\{\left[a_6 a_7 l W_{cp} P_{sm}^{l-1}\right.\right.\\ &\quad + (a_5 + a_6 P_{sm}^l)a_7 \frac{\partial W_{cp}}{\partial P_{sm}}\\ &\quad \left.-(a_9 - a_8)\right] W_{cp} + \frac{\partial W_{cp}}{\partial w_{cp}}\left[-a_1 w_{cp}\right.\\ &\quad \left.\left. - \frac{1}{w_{cp}}(a_3 P_{sm}^l - a_4)W_{cp}\right]\right\},\\ g(p) &= (a_5 + a_6 P_{sm}^l)a_2 a_7 \frac{\partial W_{cp}}{\partial w_{cp}}.\end{aligned} \tag{7}$$

2.3 | Disturbance observer

Modeling errors due to $d(t)$ negatively impact the stability and tracking performance of the controller. Therefore, to improve the accuracy of the control-oriented air-feed system model, a linear extended state observer (ESO) [26,27] is applied to estimate $d(t)$. The design of ESO follows a general way as discussed in [28].

We define $z_1 = y$, $z_2 = \dot{y}$ and an extended state $z_3 = d(t)$. Then, equation (6) can be rewritten as the following state-space equations:

$$\begin{aligned}\dot{z}_1 &= z_2,\\ \dot{z}_2 &= f_1(p)z_2 + f_2(y,p)z_1 + f_3(p) + g(p)u + z_3,\\ \dot{z}_3 &= h(t),\end{aligned} \tag{8}$$

where $h(t)$ is assumed to be an unknown term.

Then, we define the estimation error as $\tilde{z}_1 = z_1 - \hat{z}_1$. Thus, the linear ESO can be described by

$$\begin{aligned}\dot{\hat{z}}_1 &= \hat{z}_2 + 3w_o\tilde{z}_1,\\ \dot{\hat{z}}_2 &= f_1(p)\hat{z}_2 + f_2(y,p)\hat{z}_1 + f_3(p) + g(p)u + \hat{z}_3 + 3w_o^2\tilde{z}_1,\\ \dot{\hat{z}}_3 &= w_o^3\tilde{z}_1,\end{aligned} \tag{9}$$

where $[3w_o \quad 3w_o^2 \quad w_o^3]$ is the vector of the observer gains as suggested in [28] where w_o is tuned according to the convergence time. Hence, $d(t)$ is estimated by

$$\hat{d}(t) = \hat{z}_3. \tag{10}$$

The main contribution of the ESO is to improve the modeling accuracy of fuel cell model and extend the application of triple-step method to a specific system with certain modeling uncertainties as discussed in section 3.

Combining (6) with the estimated disturbance in (10), the control-oriented model is written as

$$\ddot{y} = f_1(p)\dot{y} + f_2(y,p)y + f_3(p) + g(p)u + \hat{d}(t). \tag{11}$$

Note that the delicately designed control-oriented model (11) is with an affine formulation which facilitates the controller design by applying the triple-step method as discussed in section 3. However, the modeling procedure is not unique, any delicately designed model which is able to describe the system input and output with an affine form will fit for the triple step method.

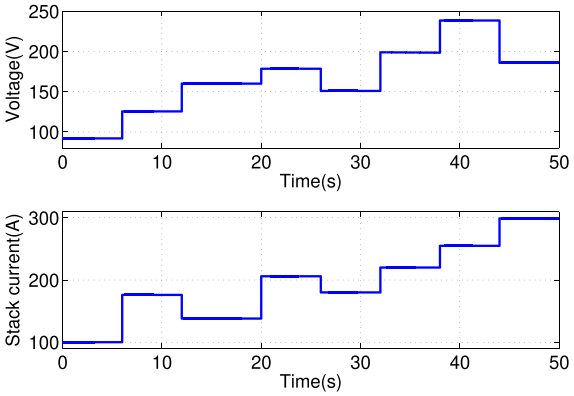

FIGURE 2 Stepwise changes in voltage and stack for current for model validation [Color figure can be viewed at wileyonlinelibrary.com]

2.4 | Model validation

The high fidelity model developed in [5] is used as the plant model for model validation. The control input u and the exogenous input are set as step changed signals as shown in Figure 2. The modeling verification and the effectiveness of ESO are shown in Figure 3 and Figure 4. It can be seen that the ESO effectively estimates the modeling errors and substantially improve the modeling accuracy. Note that the initial condition of z_1 in ESO is usually set as the same as the plant model since the pressure difference, $P_{sm} - P_{ca}$, can be calculated accurately by the measured oxygen mass flow, $W_{O_2,in}$, and supply manifold pressure, P_{sm}, according to (3). The initial condition impact on the observer is shown in Figure 5 assuming that the sensors drift with a certain deviation in practice. It can be seen that the observer is sensitive to the initial value deviation where it needs a short period of warm-up time to reach the convergence. For a case study considering $2000Pa$ deviation, the adjusting time is less than 0.2s.

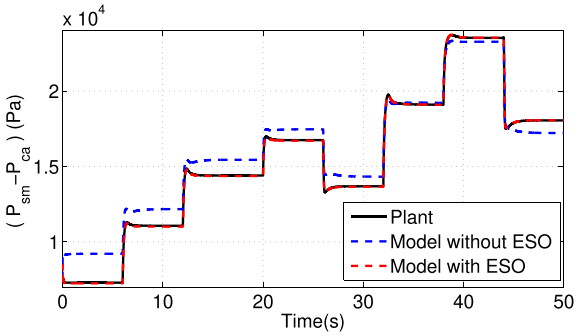

FIGURE 3 Model validation results for pressure difference $P_{sm} - P_{ca}$ [Color figure can be viewed at wileyonlinelibrary.com]

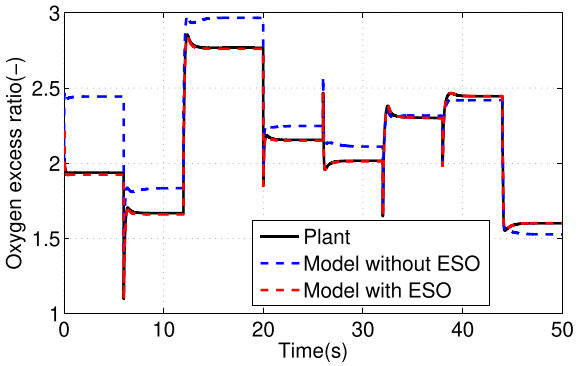

FIGURE 4 Model validation results for the oxygen excess ratio [Color figure can be viewed at wileyonlinelibrary.com]

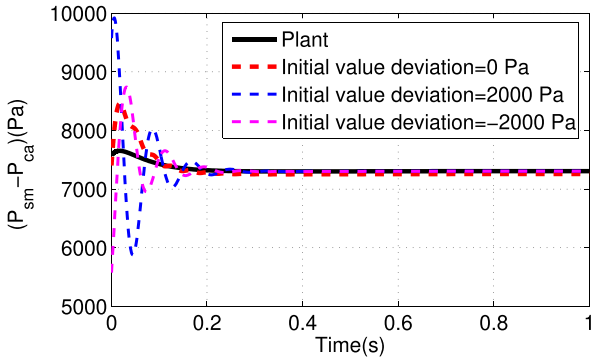

FIGURE 5 Initial condition sensitivity to the ESO [Color figure can be viewed at wileyonlinelibrary.com]

3 | ROBUST NONLINEAR TRIPLE-STEP CONTROLLER DESIGN

In this section, a nonlinear robust triple-step method is proposed for the controller design for the air-feed system. The triple step method was firstly developed to address rail pressure control problem in a gasoline direct injection engine [29] and later successfully applied to wide variety of fields over automotive control system, e.g. transmission control [20], vehicle dynamic control [30], et al. For oxygen access ratio tracking control, the proposed controller design followed by the triple-step method consists of three parts: steady-state-like control, reference-variation-based feed-forward control and robust error feedback control. The detailed controller design procedure is described as follows.

3.1 | Controller design

Step 1: Steady-state-like control. Motivated by the map-based control strategy that is widely used in modern automotive application, we first set $\ddot{y} = 0$ and $\dot{y} = 0$ in (11). Then, a steady-state-like control law can be obtained as

$$u_s = -\frac{1}{g(p)}[f_2(y,p)y + f_3(p) + \hat{d}(t)]. \tag{12}$$

The control law, u_s, depends on the control output y and the measurable state vector p.

Remark 3.1. In normal fuel cell operating condition, since $\frac{\gamma R_a k_{SM,out} T_a}{V_{SM}} a_2 a_7 \neq 0$ and $[1 - \frac{1}{\eta_{cp}} + (\frac{P_{sm}}{P_a})^l] \neq 0$, and the air mass flow rate W_{cp} is monotonous associated with compressor angular speed ω_{cp}, $\frac{\partial W_{cp}}{\partial w_{cp}} \neq 0$, thus, it is true that $g(p) \neq 0$.

Step 2: Reference-variation-based feed-forward control. Applying the steady-state-like control only is not enough to achieve satisfying performance if the system dynamics transits through different operating points. Reference variations of the control system needs to be considered. Hence, retaining the steady-state-like control, we augment the control as

$$u = u_s + u_f, \tag{13}$$

where u_f is to be determined.

By substituting (12) and (13) into (11), the model can be rewritten as

$$\ddot{y} = f_1(p)\dot{y} + g(p)u_f. \tag{14}$$

By setting $\ddot{y} = \ddot{y}^*$ and $\dot{y} = \dot{y}^*$ in (14), we obtain the following feed-forward control law,

$$u_f = \frac{1}{g(p)}\left(\ddot{y}^* - f_1(p)\dot{y}^*\right). \tag{15}$$

Step 3: Robust error feedback control. Following the two steps described above, the tracking error has not been considered. To guarantee closed-loop stability and the robustness of the system, a robust error feedback control law is subsequently derived.

We introduce a new control action u_e into the control input (13). Thus, the control input becomes

$$u = u_s + u_f + u_e. \tag{16}$$

Then, by substituting (12), (15) and (16) into (11), the model can be rewritten as

$$\ddot{y} = f_1(p)\dot{y} + \ddot{y}^* - f_1(p)\dot{y}^* + g(p)u_e + d(t) - \hat{d}(t). \tag{17}$$

We define the reference tracking error and the compensated disturbance, respectively, as

$$\begin{aligned} e &= y^* - y, \\ \tilde{d}(t) &= \hat{d}(t) - d(t). \end{aligned} \tag{18}$$

Then, we substitute (18) into (17) to obtain the tracking error dynamics as

$$\ddot{e} = f_1(p)\dot{e} - g(p)u_e + \tilde{d}(t). \tag{19}$$

To restrain the steady-state error of the system, an error integration term is introduced. We define $e_1 = e$, $e_2 = \dot{e}$ and $\chi = \int e_1 dt$, and then the error state equation follows

$$\begin{aligned} \dot{e}_1 &= e_2, \\ \dot{e}_2 &= f_1 p e_2 - g(p)u_e + \tilde{d}(t). \end{aligned} \tag{20}$$

For (20), a specific Lyapunov function is selected as

$$V_1 = \frac{k_1}{2}\chi^2 + \frac{1}{2}e_1^2. \tag{21}$$

Differentiating the Lyapunov function (21) with respect to time, yields

$$\dot{V}_1 = k_1\chi^2 e_1 + e_1 e_2 = e_1(k_1\chi + e_2). \tag{22}$$

We enforce $k_1\chi + e_2 = -k_2 e_1$ and $k_2 > 0$ to satisfy

$$\dot{V}_1 = -k_2 e_1^2 \leq 0, \tag{23}$$

where the equality situation $\dot{V}_1 = 0$ only occurs when $e_1 = 0$ [31]. Then, we can obtain

$$e_2 = -k_1\chi - k_2 e_1 \triangleq e_{2d}. \tag{24}$$

To ensure that e_2 is asymptotically stable and converges to e_{2d}, we define a new error state $e_3 = e_{2d} - e_2$. Then, an additional Lyapunov function is defined as

$$V_2 = V_1 + \frac{1}{2}e_3^2. \tag{25}$$

By differentiating (25), we can infer

$$\begin{aligned} \dot{V}_2 &= \dot{V}_1 + e_3(\dot{e}_2 - \dot{e}_{2d}) \\ &= e_1(k_1\chi + e_2) + e_3[f_1(p)e_2 - g(p)u_e - \dot{e}_{2d} + \tilde{d}(t)] \\ &= e_1(k_1 + e_{2d} + e_3) + e_3[f_1(p)e_2 - g(p)u_e - \dot{e}_{2d} + \tilde{d}(t)] \\ &= e_1(k_1 + e_{2d}) + e_3[e_1 + f_1(p)e_2 - g(p)u_e - \dot{e}_{2d}] + e_3\tilde{d}(t) \\ &\leqslant -k_2 e_1^2 + e_3[e_1 + f_1(p)e_2 - g(p)u_e - \dot{e}_{2d}] + e_3\mathrm{sign}(e_2)\tilde{d}_{\max} \\ &= -k_2 e_1^2 + e_3[e_1 + f_1(p)e_2 - g(p)u_e - \dot{e}_{2d} + \mathrm{sign}(e_3)\tilde{d}_{\max}], \end{aligned} \tag{26}$$

where $\tilde{d}_{\max} = \sup \tilde{d}(t)$.

We further enforce $e_1 + f_1(p)e_2 - g(p)u_e - \dot{e}_{2d} + \mathrm{sign}(e_2)\tilde{d}_{\max} = -k_3 e_3$, then (26) can be represented as

$$\dot{V}_2 \leqslant -k_2 e_1^2 - k_3 e_3^2. \tag{27}$$

With the choice of $k_3 > 0$, the closed-loop tracking error system is asymptotically stable [32].

Hence, a robust error feedback control law can be written as follows:

$$u_e = \frac{1}{g(p)}[k_3 e_3 + e_1 + f_1(p)e_2 - \dot{e}_{2d} - \mathrm{sign}(e_3)\tilde{d}_{\max}]. \tag{28}$$

By substituting $\chi = \int e_1 dt, \dot{e}_1 = e_2$ and $\dot{e}_{2d} = -k_1 e_1 - k_2 \dot{e}_1$ into (28), the error feedback control law is given as

$$u_e = \frac{k_1 + k_2 + 1}{g(p)} e_1 + \frac{k_1}{g(p)} \int e_1 dt + \frac{f_1(p) + k_1 + 1}{g(p)} \dot{e}_1 - \frac{1}{g(p)} \text{sign}(e_3) \tilde{d}_{\max}. \tag{29}$$

By combining (12), (15) and (29), the overall control law is summarized as

$$u = u_s + u_f + f_P(p) e_1 + f_I(p) \chi + f_D \dot{e}_1 - \frac{\tilde{d}_{\max}}{g(p)} \text{sign}(e_3), \tag{30}$$

with

$$\begin{aligned} u_s &= -\frac{1}{g(p)} (f_2(y,p) y + f_3(p) + \hat{d}(t)), \\ u_f &= \frac{1}{g(p)} (\ddot{y}^* - f_1(p) \dot{y}^*), \\ f_P(p) &= \frac{k_1 + k_2 + 1}{g(p)}, \\ f_I(p) &= \frac{k_1}{g(p)}, \\ f_D(p) &= \frac{f_1(p) + k_1 + 1}{g(p)}. \end{aligned} \tag{31}$$

The structural schematics of the proposed control law is shown in Figure 6. The metrics of the proposed control law is described as follows. Firstly, when the system reaches a steady state, the steady-state control u_s dominates the regulation. Secondly, considering the reference variation, the feed-forward control law u_f provides an anticipatory control action which helps to improve the transient tracking performance. Thirdly, after extracting some of the system nonlinearities through step 1 and step 2, we obtain an explicit and affine expression for the error state system where an error feedback law can be intuitively designed with gain scheduling characteristics. The proposed controller is concise and comparable to the structure adopted for modern automotive control in practice. Although it does require modelling efforts, it has significant advantages in reducing the calibration workload and improving the transient control performance. Overall, it helps to bridge the gap between theoretical nonlinear control methodologies and the corresponding engineering implementations.

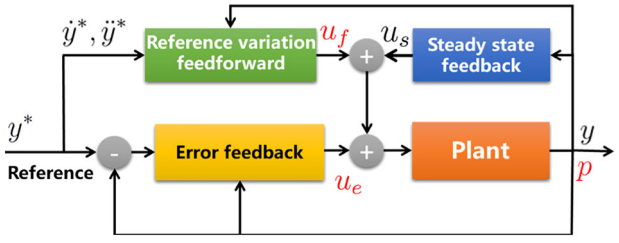

FIGURE 6 Schematics of the proposed triple-step control law [Color figure can be viewed at wileyonlinelibrary.com]

3.2 | Guideline for the control parameter tuning rules

Substituting (24) and (30) into (11), the closed-loop error system is obtained as

$$\begin{aligned} \dot{\chi} &= e_1, \\ \dot{e}_1 &= -k_1 \chi - k_2 e_1 - e_3, \\ \dot{e}_3 &= e_1 - k_3 e_3 + d', \end{aligned} \tag{32}$$

where $d' = \hat{d}(t) - \text{sign}(e_3) d_{\max}$ is the bounded disturbance in the closed-loop error system.

From (32), it is indicated that k_2 dominates the decay of the tracking error e_1 and k_3 dominates the decay for e_3. Based on this consideration, k_1 and k_2 should be chosen as large as possible. However, from (30) and (31), excessively large k_1 and k_2 values will result in high gain issue which should be dealt with carefully in practice.

In the following, we determine a specific guideline for tuning rule by analyzing the tracking error under linear control theory framework. Applying Laplace transformation [33] to (32) to obtain the transfer function of the tracking error,

$$E_1(s) = \frac{1}{(s + k_2 + \frac{k_1}{s})(s + k_3) + 1} D'(s). \tag{33}$$

Through the use of the final-value theorem [34], we can calculate the tracking offset as

$$E_1(\infty) = \lim_{s \to 0} s \left[\frac{1}{(s + k_2 + \frac{k_1}{s})(s + k_3) + 1} D'(s) \right]. \tag{34}$$

In such a case, the tracking error directly depends on the disturbance d'. If d' is an impulse signal or a step signal, $e_1(\infty) = 0$. If d' is a ramp signal with a slope, $\bar{d}'$, then the tracking offset becomes

$$E_1(\infty) = \frac{\bar{d}'}{k_1 k_3}. \tag{35}$$

In general, with limited knowledge of disturbances, $k_1 k_3$ tends to be selected as a sufficiently large number to reduce the tracking offset. As a summary, we can follow the guidelines for parameters tuning as below:

- Choose k_2 in accordance with the required decay rate of e_1, where a large k_2 value corresponds to a fast decay rate;
- Choose a large k_1 value to achieve an acceptable tracking offset;

- Choose $k_2 \leq k_1$ for a trade-off between fast response and oscillation while avoiding the potential high gain.

4 | IMPLEMENTATION ISSUES AND SIMULATION RESULTS

In this section, potential issues towards implementation are addressed and the performance of the proposed control scheme is validated via simulation study.

4.1 | Implementation issues

For practical implementation, we introduce a method for signal processing and the calculation of the derivatives which are necessary for the proposed control scheme.

According to (4), the reference y^* can be calculated from the reference oxygen excess ratio $\lambda^*_{O_2}$ as,

$$y^* = \frac{c_2 I_{st}}{c_1} \lambda^*_{O_2}, \tag{36}$$

where $\lambda^*_{O_2} = 2$ is a conventional setup to maximize the output power of a PEMFC.

To obtain $\dot{y}^*$ and $\ddot{y}^*$ from the reference trajectory y^*, low-pass filters [35] can be used for the signal processing. Let the reference be denoted by $\bar{y}^*$. By passing $\bar{y}^*$ through a second-order filter, one can obtain

$$\frac{y^*}{\bar{y}^*} = \frac{w_n^2}{s^2 + 2\xi w_n s + w_n^2}. \tag{37}$$

The block diagram of this second-order filter is shown in Figure 7. Both $\dot{y}^*$ and $\ddot{y}^*$ are obtained as presented in this figure.

4.2 | Simulation results and analysis

The effectiveness of the proposed controller is validated and compared with two PID controllers in a high fidelity plant model developed in [5]. The PID controller is defined as

$$u_{pid} = K_p e_\lambda(t) + K_i \int e_\lambda(t) dt + K_d \frac{de_\lambda(t)}{dt}, \tag{38}$$

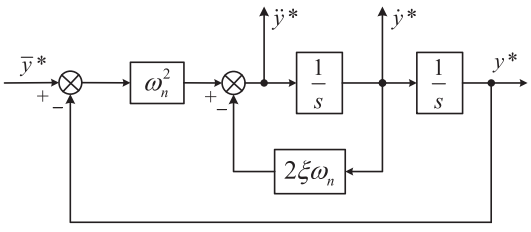

FIGURE 7 Schematics of the second-order filter for input shaping [Color figure can be viewed at wileyonlinelibrary.com]

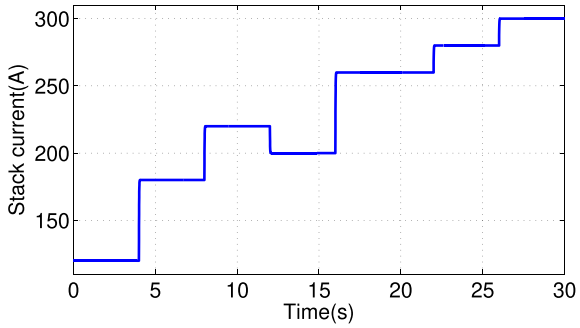

FIGURE 8 Step changing stack current [Color figure can be viewed at wileyonlinelibrary.com]

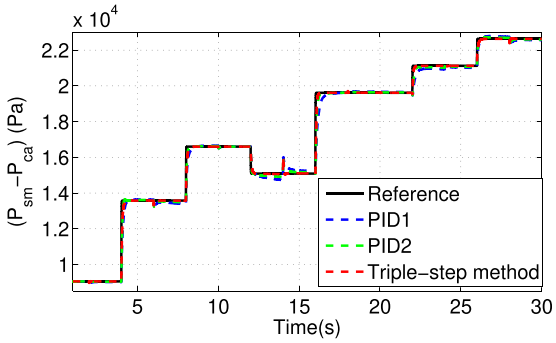

FIGURE 9 Simulation result for $P_{sm} - P_{ca}$ tracking: transient testing with nominal model parameters [Color figure can be viewed at wileyonlinelibrary.com]

where $e_\lambda = \lambda^*_{O_2} - \lambda_{O_2}$. Note that the oxygen access ratio is directly selected as the control output for PID controller to make a ideal baseline controller for the subsequent comparisons. To verify of the effectiveness of the proposed nonlinear controller, two PID controllers with different well tuned control gains are considered. The first "PID1" controller is designed to avoid tracking oscillation while achieving fast adjustment, where $K_p = 80$, $K_i = 1000$ and $K_d = 0.2$. By contrast, the second "PID2" pursues for the fast adjustment with a small overshoot where $K_p = 80$, $K_i = 650$ and $K_d = 0.2$. The parameter of the disturbance observer is set as $w_o = 100$. In accordance with the proposed controller parameter tuning rule, the parameters of the proposed controller are set to $k_1 = 15000$, $k_2 = 1000$ and $k_3 = 50$.

To demonstrate the transient tracking performance of the robust triple-step method, it is assumed that the PEMFC system is operating with step-wise changed stack current as shown in Figure 8. Figure 9 and Figure 10 present the control performance in terms of pressure difference, $P_{sm} - P_{ca}$, and the oxygen excess ratio, λ_{O_2}, respectively. Figure 11 and Figure 12 show the zoom-in plots in the time window of $3.5 - 5s$ accordingly. As shown in Figure 9-Figure 10, the robust triple-step method can track the oxygen excess ratio set-point faster with less overshoot

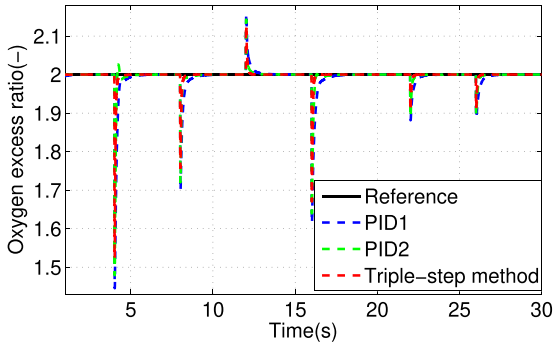

FIGURE 10 Simulation results for the oxygen excess ratio: transient testing with nominal model parameters [Color figure can be viewed at wileyonlinelibrary.com]

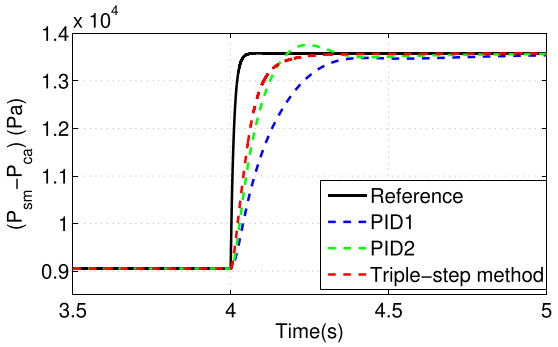

FIGURE 11 Zoom-in plot for $P_{sm} - P_{ca}$ tracking during 3.5-5 s: transient testing with nominal model parameters [Color figure can be viewed at wileyonlinelibrary.com]

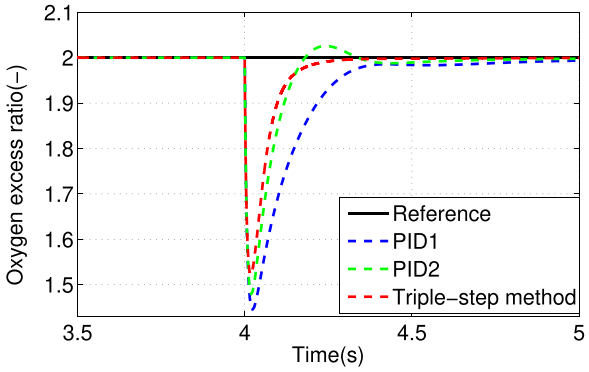

FIGURE 12 Zoom-in plot for oxygen excess ratio during 3.5-5 s: transient testing with nominal model parameters [Color figure can be viewed at wileyonlinelibrary.com]

compared with both of the two PID controllers. Apparently, the fast transient performance of the nonlinear controller is benefited by the applied reference variation-based feedforward control and the feedback control with scheduled gains depending transient states. By contrast, the "PID1" controller is able to track the desired set-point without oscillations, but it requires the longest time to converge

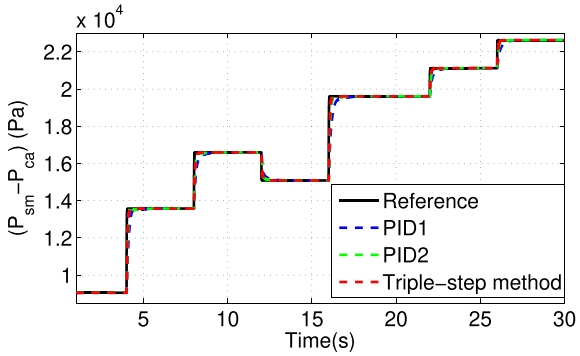

FIGURE 13 Simulation result for $P_{sm} - P_{ca}$ tracking: testing with perturbed stack temperature [Color figure can be viewed at wileyonlinelibrary.com]

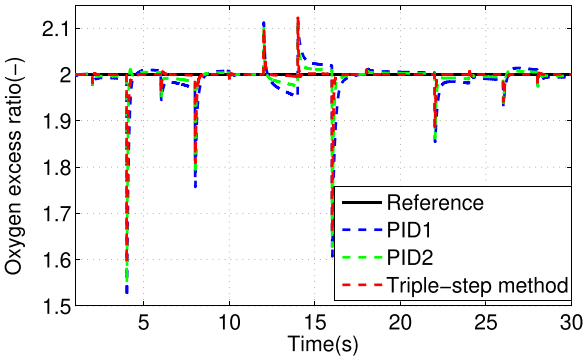

FIGURE 14 Simulation result for the oxygen excess ratio: testing with perturbed stack temperature [Color figure can be viewed at wileyonlinelibrary.com]

and has the largest overshoot. The "PID2" can achieve rapid regulation, however, generates oscillations.

Next, the performances of robustness against parameter varying condition are compared. In practice, parameters, e.g. stack temperature, of PEMFCs may vary under different operating conditions. In the simulation, we assume the stack temperature is perturbed by Gaussian noise disturbance where the mean is $353K$ and the variance is $20K$. As shown in Figure 13 and Figure 14, for "PID1" and "PID2" controllers, the oxygen excess ratios deviate from the desired value in steady state due to stack temperature drifts, whereas the proposed nonlinear controller achieves very small steady-state error.

Overall, the proposed nonlinear controller has very good tracking performance in transients and has robustness against certain parameter drift.

5 | CONCLUSION

This paper proposes a robust nonlinear controller for oxygen access ratio tracking control in the air-feed system of a PEMFC. A control-oriented model is introduced

that represents oxygen access behavior as an input-output affine-like dynamic system where an ESO is collaborated to compensate system uncertainties and disturbances. Facilitated by the delicately derived control-oriented model, a nonlinear robust controller is designed to stabilize the system based on triple step method including a steady-state like control, a reference-variation-based feedforward control and an error feedback control. A specific control tuning rule is carried out in the scheme of linear control theory. The simulation results conducted in a high fidelity model demonstrate that the proposed controller achieves good transient tracking performance and robustness against parameter drift. Future work will focus on the development of a test-bench and the experimental validation of the controller.

ACKNOWLEDGEMENTS

This work was supported by National Natural Science Foundation of China (No. 61703177, 11601040), Jilin Provincial Science Foundation of China (No. 20190302119GX, 20180101037JC), Jilin Provincial Development and Reform Commission Foundation of China (No. 2019C036-4) and Funds for Joint Project of Jilin Province and Jilin University under Grant No. SXGJSF2017-2-1-1.

ORCID

Yunfeng Hu https://orcid.org/0000-0003-4068-0664
Jinwu Gao https://orcid.org/0000-0003-2745-1920

REFERENCES

1. J. Li, C. Fang, and L. Xu, *Current status and trends of the research and development for fuel cell vehicles*, J. Autom. Saf. Energy **5** (2014), 17–29.
2. B. Wu, M. Matian, and G. J. Offer, *Hydrogen PEMFC system for automotive applications*, Int. J. Low-Carbon Technol. **7** (2012), no. 1, 28–37.
3. N. Mebarki et al., *PEM Fuel cell/battery storage system supplying electric vehicle*, Int. J. Hydrogen Energy **41** (2016), no. 45, 20993–21005.
4. W. R. W. Daud et al., *PEM Fuel cell system control: A review*, Renew. Energy **113** (2017), 620–638.
5. J. T. Pukrushpan, AG Stefanopoulou, and H. Peng, *Control of Fuel Cell Power Systems: Principles, Modeling, Analysis and Feedback Design*, Springer Science & Business Media, London, 2004.
6. L. Xu, J. Li, and M. Ouyang, *Energy flow modeling and real-time control design basing on mean values for maximizing driving mileage of a fuel cell bus*, Int. J. Hydrogen Energy **40** (2015), no. 43, 15052–15066.
7. M. Gerard et al., *Oxygen starvation analysis during air feeding faults in PEMFC*, Int. J. Hydrogen Energy **35** (2010), no. 22, 12295–12307.
8. Y. Tang et al., *Experimental investigation of dynamic performance and transient responses of a kW-class PEM fuel cell stack under various load changes*, Appl. Energy **87** (2010), no. 4, 1410–1417.
9. Z. Baroud et al., *Novel hybrid fuzzy-PID control scheme for air supply in PEM fuel-cell-based systems*, Int. J. Hydrogen Energy **42** (2017), no. 15, 10435–10447.
10. C. Damour et al., *Real-time implementation of a neural model-based self-tuning PID strategy for oxygen stoichiometry control in PEM fuel cell*, Int. J. Hydrogen Energy **39** (2014), no. 24, 12819–12825.
11. H. Beirami, A. Z. Shabestari, and M. M. Zerafat, *Optimal PID plus fuzzy controller design for a PEM fuel cell air feed system using the self-adaptive differential evolution algorithm*, Int. J. Hydrogen Energy **40** (2015), no. 30, 9422–9434.
12. M. Becherif and D. Hissel, *MPPT of a PEMFC based on air supply control of the motocompressor group*, Int. J. Hydrogen Energy **35** (2010), no. 22, 12521–12530.
13. C. Bao, M. Ouyang, and B. Yi, *Modeling and control of air stream and hydrogen flow with recirculation in a PEM fuel cell system–II. Linear and adaptive nonlinear control*, Int. J. Hydrogen Energy **31** (2006), no. 13, 1897–1913.
14. A. Arce et al., *Real-time implementation of a constrained MPC for efficient airflow control in a PEM fuel cell*, IEEE Trans. Ind. Electron. **57** (2010), no. 6, 1892–1905.
15. C. Kunusch et al., *Experimental results applying second order sliding mode control to a PEM fuel cell based system*, Control Eng. Practice **21** (2013), no. 5, 719–726.
16. D. Zhao et al., *Sliding-mode control of an ultrahigh-speed centrifugal compressor for the air management of fuel-cell systems for automotive applications*, IEEE Trans. Veh. Technol. **63** (2014), no. 1, 51–61.
17. L. Xu et al., *Robust control of internal states in a polymer electrolyte membrane fuel cell air-feed system by considering actuator properties*, Int. J. Hydrogen Energy **42** (2017), no. 18, 13171–13191.
18. R. J. Talj et al., *Experimental validation of a PEM fuel-cell reduced-order model and a moto-compressor higher order sliding-mode control*, IEEE Trans. Ind. Electron. **57** (2010), no. 6, 1906–1913.
19. Q. Ouyang et al., *Nonlinear MPC Controller Design for AIR Supply of PEM Fuel Cell Based Power Systems*, Asian J. Control **19** (2017), no. 3, 929–940.
20. B. Gao et al., *Position control of electric clutch actuator using a triple-step nonlinear method*, IEEE Trans. Ind. Electron. **61** (2014), no. 12, 6995–7003.
21. F. Wang, H. Chen, and D. Cao, *Nonlinear coordinated motion control of road vehicles after a tire blowout*, IEEE Trans. Control Syst. Technol. **24** (2016), no. 3, 956–970.
22. H. Chu et al., *Low-speed control for permanent-magnet DC torque motor using observer-based nonlinear triple-step controller*, IEEE Trans. Ind. Electron. **64** (2017), no. 4, 3286–3296.
23. S. J. Peighambardoust, S. Rowshanzamir, and M. Amjadi, *Review of the proton exchange membranes for fuel cell applications*, IEEE Trans. Ind. Electron. **35** (2010), no. 17, 9349–9384.
24. F. Wang et al., *Feedback linearization control of the air supply system of PEM fuel cells*, 2015 10th Asian Control Conference (ASCC), Kota Kinabalu, Malaysia, 2015, pp. 1–6.
25. T. Zhang et al., *A review of automotive proton exchange membrane fuel cell degradation under start-stop operating condition*, Appl. Energy **223** (2018), 249–262.
26. M. R. Mokhtari, A. C. Braham, and B. Cherki, *Extended State Observer based control for coaxial-rotor UAV*, ISA Trans. **61** (2016), 1–14.

27. S. Xingling and W. Honglun, *Trajectory linearization control based output tracking method for nonlinear uncertain system using linear extended state observer*, Asian J. Control **18** (2016), no. 1, 316–327.
28. Q. Zheng, L. Q. Gao, and Z Gao, *On validation of extended state observer through analysis and experimentation*, J. Dyn. Syst., Meas., Control **134** (2012), no. 2, 24505.
29. H. Chen et al., *Triple-step method to design non-linear controller for rail pressure of gasoline direct injection engines*, IET Control Theory Appl. **8** (2014), no. 11, 948–959.
30. H. Zhao, *Integrated control of in-wheel motor electric vehicles using a triple-step nonlinear method*, J. Franklin Institute **352** (2015), no. 2, 519–540.
31. H. J. Marquez, *Nonlinear control systems: Analysis and design*, 1st ed., Wiley-Interscience, Hoboken, NJ, 2003.
32. H. K. Khalil, *Nonlinear systems*, 3rd ed., Prentice Hall, Upper Saddle River, NJ, 2002.
33. W. J. Rugh and W. J. Rugh, *Linear system theory*, 2nd ed., Prentice Hall, Upper Saddle River, NJ, 1996.
34. R. C. Dorf and R. H. Bishop, *Modern control systems*, Eleventh Edition, Prentice Hall, Upper Saddle River, NJ, 2007.
35. D. Ahn et al., *A design of the low-pass filter using the novel microstrip defected ground structure*, IEEE Trans. Microw. Theory Tech. **49** (2001), no. 1, 86–93.

AUTHOR BIOGRAPHIES

Yunfeng Hu received the M.S. degree in basic mathematics and the Ph.D. degree in control theory and control engineering from Jilin University, Changchun, China, in 2008 and 2012, respectively.

He is currently an Associate Professor with the Department of control Science and Engineering, Jilin University. His current research interests include nonlinear control and automotive control.

Huan Chen received the B.S. degree in control theory and control engineering from Jilin University, Changchun, China, in 2016. She is currently a M.S. student with the Department of control Science and Engineering, Jilin University. Her current research interests include nonlinear control and engine control.

Xun Gong received the B.S. degree in electrical engineering from Northeast Electrical Power University, in 2010, and the the Ph.D. degree in control theory and control engineering from Jilin University, in 2016. He was a joint Ph.D. student and a postdoctoral researcher in the University of Michigan, Ann Arbor, from 2013 to 2015 and 2016 to 2018 respectively. His current research interests include model-based nonlinear control and optimal control, and control applications to automotive systems.

Shuyou Yu received the B.S. and M.S. degrees in Control Science & Engineering at Jilin University, PR China, in 1997 and 2005, respectively, and the Ph.D. degree in Engineering Cybernetics at the University of Stuttgart, Germany, in 2011. From 2010 to 2011, he was a research and teaching assistant at the Institute for Systems Theory and Automatic Control at the University of Stuttgart. In 2012, he joined the faculty of the Department of Control Science & Engineering at Jilin University, PR China, where he is currently a full professor.

His main areas of interest are in model predictive control, robust control, and applications in mechatronic systems.

Jinwu Gao received the B.Eng. degree in the Department of Automation Measurement and Control Engineering, and the Ph.D. degree in the Department of Control Science and Engineering from Harbin Institute of Technology, Harbin, China, in 2005 and 2012.

From 2012 to 2014, he was an Assistant Professor at Sun Yat-sen University, China. In July 2014, he held postdoctoral position in the Department of Engineering and Applied Science, Sophia University, Japan. Since November 2016, he has been an Associate Professor at Jilin University, China. His research interests include control theory and application in automotive powertrain.

Hong Chen (M'02-SM'12) received the Ph.D. degree in system dynamics and control engineering from the University of Stuttgart, Stuttgart, Germany, in 1997.

She joined Jilin University, Changchun, China, in 1986, where she became an Associate Professor in 1998 and has been a Professor since 1999. Her current research interests include model predictive control, optimal and robust control, and applications in process engineering and mechatronic systems.

How to cite this article: Hu Y, Chen H, Gong X, Yu S, Gao J, Chen H. Control-oriented modeling and robust nonlinear triple-step controller design for an air-feed system for polymer electrolyte membrane fuel cells. *Asian J Control*. 2019;21: 1811–1823. https://doi.org/10.1002/asjc.2146

APPENDIX A

$$a_1 = \frac{\eta_{cm} k_t k_v}{J_{cp} R_{cm}},\ a_2 = \frac{\eta_{cm} k_t}{J_{cp} R_{cm}},\ a_3 = \frac{C_p T_a}{J_{cp} \eta_{cp} (P_a)^{\frac{\gamma-1}{\gamma}}},$$

$$a_4 = \frac{C_p T_a}{J_{cp} \eta_{cp}}, l = \frac{\gamma - 1}{\gamma},\ a_6 = \frac{\gamma R_a T_a K_{sm,out}}{V_{sm} \eta_{cp} (P_a)^{\frac{\gamma-1}{\gamma}}},$$

$$a_5 = \frac{\gamma R_a T_a K_{sm,out}}{V_{sm}} (1 - \frac{1}{\eta_{cp}}),\ a_7 = \frac{1}{K_{sm,out}},$$

$$a_8 = \frac{R_a T_{st}}{V_{ca}} \left[\frac{K_{sm,out}}{M_a (1 + \Omega)} + \frac{C_D A_T \gamma^{\frac{1}{2}}}{\kappa \sqrt{R_a T_{st}}} \left(\frac{2}{\gamma + 1} \right)^{\frac{\gamma+1}{2(\gamma-1)}} \right],$$

$$a_9 = \frac{R_a T_{st}}{V_{ca}} \frac{K_{sm,out}}{M_a (1 + \Omega)},\ a_{11} = \frac{n R_a T_{st}}{4 F V_{ca}},$$

$$a_{10} = \frac{R_a T_{st}}{V_{ca}} \frac{C_D A_T \gamma^{\frac{1}{2}}}{\kappa \sqrt{R_a T_{st}}} \left(\frac{2}{\gamma + 1} \right)^{\frac{\gamma+1}{2(\gamma-1)}} P_{sat},$$

$$\alpha_1 = B b_1,\ \alpha_2 = B b_2 A,\ \alpha_3 = B b_3 A^2,$$

$$\alpha_4 = B b_4 A^3,\ \beta = b_6 A^2 w_{cp}^2 + b_7 A w_{cp} + b_8,$$

$$\alpha_5 = B b_5 A^4,\ \psi = \frac{C_p T_a \left[\left(\frac{P_{ca}}{P_a} \right)^{\frac{\gamma-1}{\gamma}} - 1 \right]}{\frac{1}{2} \left(\frac{\pi}{60} \sqrt{\frac{T_{rf}}{T_a}} w_{cp} \right)^2},$$

$$\psi_{max} = b_9 A^5 w_{cp}^5 + b_{10} A^4 w_{cp}^4 + b_{11} A^3 w_{cp}^3 + b_{12} A^2 w_{cp}^2 + b_{13} A w_{cp} + b_{14},$$

$$\Omega = \frac{M_v \phi_a P_{sat}}{M_a (P_a - \phi_a P_{sat})},\ A = \frac{\pi d_c}{\sqrt{\gamma R_a T_a}} \sqrt{\frac{T_{rf}}{T_a}},$$

$$B = \frac{\pi^2 d_c^3 \rho_a P_a T_{rf}}{240 T_a P_{rf}},\ c_1 = \frac{x_{O_2,in} K_{sm,out}}{1 + \Omega},$$

$$c_2 = \frac{n M_{O_2}}{4F}.$$

TABLE A1 Compressor regression coefficients

Symbol	Value
κ	25.85×10^{-3}
b_1	2.21×10^{-3}
b_2	-4.64×10^{-5}
b_3	-5.36×10^{-4}
b_4	2.70×10^{-4}
b_5	-3.70×10^{-5}
b_6	1.76567
b_7	−1.34837
b_8	2.44419
b_9	-9.78755×10^{-3}
b_{10}	0.10581
b_{11}	−0.42937
b_{12}	0.80121
b_{13}	−0.68344
b_{14}	0.43331

TABLE A2 General parameters used for modeling

Symbol	Parameter	SI units	Value
η_{cm}	Mechanical efficiency of the compressor motor	–	0.98
k_t	Motor constant	Nm/A	0.0153
k_v	Motor constant	$V/(rad/s)$	0.0153
J_{cp}	Compressor and motor inertia	$kg \cdot m^2$	5×10^{-5}
R_{cm}	Motor constant	ohm	0.82
C_p	Specific heat of air	$J/kg/K$	1004
T_a	Atmospheric temperature	T_a	298.15
P_a	Atmospheric pressure	P_a	1.013×10^5
η_{cp}	Compressor efficiency	–	0.8
R_a	Gas constant of air	$J/mol/K$	286.9
γ	Specific heat ratio of air	–	1.4
$K_{sm,out}$	Supply manifold outlet orifice constant	$kg/s/Pa$	0.3629×10^{-5}
V_{sm}	Supply manifold volume	m^3	0.02
T_{st}	Temperature of the fuel-cell stack	K	353
V_{ca}	Single stack cathode volume	m^3	0.01
M_a	Molar mass of air	kg/mol	28.97×10^{-3}
C_D	Return manifold throttle discharge coefficient	–	0.0124
A_T	Return manifold throttle area	m^2	0.002
P_{sat}	Saturation pressure	P_a	-
n	Number of the cells in fuel-cell stack	–	381
F	Faraday constant	$A \cdot s/mol$	96487
ρ_a	Air density	kg/m^3	1.23
T_{rf}	Reference temperature	K	288
P_{rf}	Reference pressure	Pa	1.01325×10^5
d_c	Compressor diameter	m	0.2286
M_v	Molar mass of vapor	kg/mol	18.02×10^{-3}
ϕ_a	Average ambient relative humidity of air	–	0.5
M_{O_2}	Molar mass of oxygen	kg/mol	32.0×10^{-3}
$x_{O_2,in}$	Oxygen mole fraction at the cathode inlet	–	0.21